Carbohydrate Polymers 201 (2018) 151–161

Contents lists available at ScienceDirect

Carbohydrate Polymers

journal homepage: www.elsevier.com/locate/carbpol

Synthesis, structural and *in-vitro* characterization of β-cyclodextrin grafted *L*-phenylalanine functionalized graphene oxide nanocomposite: A versatile nanocarrier for pH-sensitive doxorubicin delivery

Sedigheh Borandeh[a,*], Amir Abdolmaleki[b,c], Samira Sadat Abolmaali[a,d], Ali Mohammad Tamaddon[a,d]

[a] Center for Nanotechnology in Drug Delivery, Shiraz University of Medical Sciences, Shiraz, Iran
[b] Department of Chemistry, Isfahan University of Technology, Isfahan, Iran
[c] Department of Chemistry, College of Sciences, Shiraz University, Shiraz, Iran
[d] Department of Pharmaceutics, School of Pharmacy, Shiraz University of Medical Sciences, Shiraz, Iran

ARTICLE INFO

Keywords:
Nanocarrier
Graphene oxide
Cyclodextrin
Drug delivery
Cytocompatibility

ABSTRACT

To enhance graphene stability, drug loading capacity and biocompatibility, β-cyclodextrin (β-CD) was grafted onto graphene oxide (GO) using *L*-plenylalanine (Phe) as a linker. The doxorubicin (DOX) loading efficiency and capacity of GO-Phe-CD were 78.7% and 85.2%, respectively. The cone shaped cavity of CD acts as a host for DOX loading through inclusion complex formation. The GO-Phe-CD nanocarrier showed higher release ratio of DOX in acidic milieu of cancer cells. In addition, general cytotoxicity of the nanocarriers was examined by MTT assay and trypan blue dye exclusion in MCF-7 cell lines. It was established that the MTT assay was not an appropriate technique for predicting the cytotoxicity of graphene based nanocarriers due to the spontaneous formation of MTT formazan by these materials; leading to a false high biocompatibility. According to the trypan blue experiment, the GO-Phe-CD had significant cytocompatibility, and the DOX-loaded GO-Phe-CD had outstanding killing capability to MCF-7 cells.

1. Introduction

Nowadays, drug nanocarriers can be considered as a bridge that links nanotechnology and drug delivery systems, which are of particular importance in clinical therapy of cancer. Among different kinds of nanocarriers, such as liposomes (Golkar, Samani, & Tamaddon, 2016), polymers (Wakaskar, 2018), nanoparticles (Karimi et al., 2017) and carbon based nanomaterials (Farvadi, Tamaddon, Sobhani, & Abolmaali, 2017), graphene derivatives have attracted much attention due to their desirable two-dimensional nanostructure containing a single layer of carbon atoms arranged in a honeycomb structure. High thermal and electrical conductivity, low cost, high strength and surface area, lack of band gap, the number of layers and lower toxicity are the unique properties that makes graphene different from other nanocarriers (Feng & Liu, 2011; Kim, Shon, Miao, Lee, & Oh, 2016; Muthoosamy, Bai, & Manickam, 2014; Zuchowska, Chudy, Dybko, & Brzozka, 2017).

The most prominent derivative of graphene is graphene oxide (GO), which consists of a wide range of oxygenated functional groups (hydroxyl, epoxy and carboxyl) on its basal plane and edges. Taking advantage of good π-π stacking and hydrophobic interactions, GO is an appropriate nanocarrier for carrying water insoluble drugs, such as anticancer ones (Duran et al., 2015; Wojtoniszak et al., 2013). However, the stability and dispersion of GO in biological solutions, such as culture medium and serum are low, leading to aggregation, that limits its applications in biomedical diagnosis and treatment (Dong et al., 2012; Hong, Compton, An, Eryazici, & Nguyen, 2012; Liu, Liu et al., 2008). Recently, efforts have been taken to improve GO solubility, stability and biocompatibility in physiological media by functionalization, especially for its usage in drug delivery system. Poly(ethylene glycol) (PEG) functionalization of GO was reported as a very useful method that effectively improves its biological dispersion and biocompatibility, which is widely used for loading and delivery of water insoluble drugs (Deb & Vimala, 2018; Liu, Robinson, Sun, & Dai, 2008). Hyaluronic acid (HA) (Yin et al., 2017), chitosan (Kumar et al., 2011; Wang et al., 2013), Pluronic F127 (Hu, Yu, Li, Zhao, & Dong, 2011), dextran (Zhang, Yang, Feng, & Liu, 2011), poly(ethylenimine) (PEI) (Yan et al., 2013) and poly (amidoamide) (PAMAM) (Makharza et al.,

* Corresponding author.
E-mail address: borandeh@sums.ac.ir (S. Borandeh).

https://doi.org/10.1016/j.carbpol.2018.08.064
Received 4 June 2018; Received in revised form 1 August 2018; Accepted 16 August 2018
Available online 17 August 2018

2013) were reported for GO functionalization in designing new drug delivery systems. Nevertheless, relative low drug loading capacity and difficult procedures have limited further use of these systems.

An alternative approach for increasing drug loading is GO functionalization with cyclodextrin (CD), a biocompatible and water-soluble oligosaccharide. CDs comprise of six, seven, and eight glucopyranose units (named α-, β-, and γ-CD, respectively). The special structure of CDs (hydrophilic external surface and hydrophobic internal cavity), enables them to bind with several molecules (like hydrophobic drugs) into their cavity to form host–guest inclusion complexes (Abdolmaleki, Mallakpour, & Borandeh, 2015; Einafshar et al., 2018; Monteil, Lecouvey, Landy, Ruellan, & Mallard, 2017). CDs can absorb many compounds into their cavity through different kinds of intermolecular interactions, including van der Waals force, hydrophobic interaction, electrostatic affinity, dipole–dipole interaction, and hydrogen bond interaction (Chen, Diao, & Zhang, 2006; Liu, Robinson et al., 2008; Vogt & Strohmeier, 2012). Therefore, functionalization of GO with CD not onaly increase the drug loading capacity, but it also improves the solubility, stability and biocompatibility of GO.

Thus, in this study, we propose a new GO based drug delivery system using β-CD moieties as modifier and *L*-phenylalanine (Phe) as a linker. The prepared GO-Phe-CD nanocarrier was structurally and morphologically characterized by Fourier transform infrared spectroscopy (FT-IR), Raman, thermogravimetric analysis (TGA), dynamic light scattering (DLS), zeta-potential, field emission scanning electron microscopy (FE-SEM) and transmission electron microscopy (TEM) techniques. Doxorubicin (DOX) was used as chemotherapeutic drug model to examine the drug-loading and releasing properties while the effect of pH was also investigated. It is expected that GO functionalization with β-CD molecules will increase the loading capacity of DOX and the controlled release of the drug. In addition, the cell cytotoxicity of GO, GO-Phe and GO-Phe-CD nanocarriers and cell killing capability with these pH-responsive DOX-loaded drug delivery systems were also carried out *via* MTT assay and trypan blue dye exclusion in MCF-7 cell lines. The obtained data were compared and discussed.

2. Experimental

2.1. Materials

Graphite powder (particle size = 70 μm, purity = 99.999%) was purchased from Merck Chemical Company (Germany). β-Cyclodextrin (β-CD), *L*-phenylalanine (Phe), potassium permanganate ($KMnO_4$), 37% hydrochloric acid (HCl), sulfuric acid (H_2SO_4), 30% hydrogen peroxide (H_2O_2), sodium nitrate ($NaNO_3$), 1,1′-carbonyldiimidazole (CDI), 3-(4,5-Dimethylthiazol-2-yl)-2,5-diphenyltetrazolium bromide (MTT) and dimethyl sulfoxide (DMSO) were all purchased from Sigma-Aldrich company and were used as received. MCF-7 cells were purchased from Pasteur Institute (Iran).

2.2. GO synthesis

Graphite was oxidized through Hummer's method (Hummers & Offeman, 1958), which describes as follow. Graphite powder (0.5 g) was poured into cold solution of concentrated H_2SO_4 (12 mL) and $NaNO_3$ (0.25 g). Then, $KMnO_4$ (1.5 g) was gradually added while stirring and cooling (the temperature of the mixture must have kept below 20 °C). The mixture was then stirred at 35 °C for 30 min and as the reaction progressed the color of the mixture turned to light brown. Then, distilled water (25 mL) was added and the temperature was raised to 98 °C for 1 h. The reaction was terminated by addition of distilled water followed by treated with 2 mL of H_2O_2 (30%) and the mixture changed into brilliant yellow color. The mixture was filtered and washed with distilled water and 10% HCl solution in order to remove metal ions. The obtained graphite oxide powder was dispersed in deionized water. The resulting yellow brownish suspension was centrifuged at 3000 rpm to eliminate unexfoliated graphitic plates. Finally, an aqueous suspension containing GO sheets was obtained through exfoliation of the filtered graphite oxide suspension through its sonication for 1 h. Finally, the resulting GO was then freeze dried and stored in vacuum for further use.

2.3. Phe functionalization of GO

Phe was attached to GO according to our previous report (Mallakpour, Abdolmaleki, & Borandeh, 2014). Briefly, GO (0.1 g) powder was dispersed in 10 mL distilled water and 10 mL solution of Phe (0.3 g) and an equimolar amount of NaOH was added. The mixture was stirred for 24 h at room temperature. The reaction was terminated by adding ethanol. The resulting precipitate was centrifuged, washed well with H_2O/EtOH mixture and finally freeze dried. In addition, to convert the carboxylate groups into carboxylic acid groups, the obtained solid was stirred and sonicated in 5% HCl solution and dried with freeze drier for 24 h.

2.4. GO-Phe-CD nanocomposite synthesis

At first 25 mg of GO-Phe was dispersed in 3 mL distilled water at room temperature. Then, CDI (25 mg) and β-CD (25 mg) were added to the suspension and the mixture was stirred for 2 h at room temperature and was sonicated for 1 h. Finally, the mixture was centrifuged at 14,000 rpm for 10 min and the precipitant was washed several times with distilled water and dried by freeze drier for 24 h.

2.5. Instrumentation

The FT-IR spectra of synthesized graphene based nanocarriers were obtained using FT-IR spectrometer (Vertex, Bruker, Germany) with a resolution of 4 cm^{-1} in range of 400–4000 cm^{-1} using KBr pellets of solid samples. Raman spectroscopy was recorded from 500 to 3500 cm^{-1} on a Almega Thermo Nicolet Dispersive Raman Spectrometer using a Nd:YLF laser source operating at wavelength of 532 nm. The thermal stability of nanocarriers were measured using Perkin-Elmer TGA7 instrument under nitrogen atmosphere at the heating rate of 10 °C/min. The morphology of GO-Phe-CD was observed using FE-SEM (HITACHI S-4160, Japan) and TEM (Philips CM 120 operated (Netherlands) at voltage of 150 kV). Hydrodynamic size and surface charge of GO, GO-Phe and GO-Phe-CD were measured based on dynamic light scattering (DLS) method using Zetasizer 3000HSA (Malvern, UK).

2.6. DOX loading

GO, GO-Phe, GO-Phe-CD (0.25 mg) were dispersed in 0.5 mL of distilled water using ultrasound irradiation. Then, DOX solution at the concentration of 1 mg/mL was added to the mixture and the pH was set to 7.4. The mixture was shaken for 72 h at room temperature in the dark. The samples were ultracentrifuged at 14,000 rpm for 30 min. The DOX concentration in the supernatant solution was measured using a standard DOX concentration curve, generated with an UV–vis-NIR spectrophotometer at the wavelength of 480 nm from a series of DOX solutions with different concentrations. The DOX loading capacity and efficiency of different nanocarriers were calculated according to the following equations:

$$\%\,DOX\ Loading\ capacity\ (LC) = \frac{mass\ of\ loaded\ DOX}{mass\ of\ nanocarrier} \times 100 \quad (1)$$

$$\%\,DOX\ Loading\ efficiency\ (LE) = \frac{Initial\ DOX\ conc. - Supernatant\ DOX\ conc.}{Initial\ DOX\ conc.} \times 100 \quad (2)$$

2.6.1. Adsorption isotherm

DOX adsorption isotherm study was carried out by 0.25 mg of GO-Phe-CD with different DOX concentrations ranging from 250 μg/mL-1000 μg/mL. To investigate DOX adsorption mechanism on GO-Phe-CD nanocarrier, four models, including Langmuir (Eq. (3)), Freundlich (Eq. (4)), Temkin (Eq. (5)) and Dubinin-Raduskevich (Eq. (6)) (Ayawei, Ebelegi, & Wankasi, 2017) were used, as follows:

$$\frac{C_e}{Q_e} = \frac{C_e}{Q_m} + \frac{1}{Q_m K_L} \tag{3}$$

where C_e is the equilibrium concentration of the solution (mg/L), Q_e is the amount of drug adsorbed per gram of the adsorbent at equilibrium (mg/g). Q_m is the maximum adsorption capacity (mg/g), k_L is a Langmuir constant related to the affinity of the binding sites and energy of adsorption (L/g), which can be obtained from the plot of C_e/Q_e *vs.* C_e.

$$LnQ_e = LnK_F + \frac{1}{n} LnC_e \tag{4}$$

where k_F is a Freundlich constant related to adsorption capacity (L/g), $1/n$ is a parameter related to adsorption intensity. The Freundlich constants can be calculated from the plots of $\mathrm{Ln}Q_e$ *vs.* $\mathrm{Ln}C_e$.

$$Q_e = \frac{RT}{b} LnK_T + \frac{RT}{b} LnC_e \tag{5}$$

where K_T is the equilibrium binding constant (L/g) corresponding to the maximum binding energy, b is Temkin isotherm constant, R is the universal gas constant (8.314 J/mol/K) and T is the temperature (K). Plotting Q_e *versus* $\mathrm{Ln}(C_e)$ results in a straight line of slope RT/b and intercept (RT ln K_T)/b.

$$LnQ_e = LnQ_s - K_D\varepsilon^2 \tag{6}$$

where Q_e is amount of adsorbate in the adsorbent at equilibrium (mg/g), Q_s is theoretical isotherm saturation capacity (mg/g), K_D is Dubinin–Radushkevich isotherm constant (mol^2/kJ^2), and ε is Dubinin–Radushkevich isotherm constant. By plotting $\mathrm{Ln}(Q_e)$ against ε^2, the Dubinin-Radushkevich constants of K_D and Q_s can be obtained.

2.7. DOX release study

DOX release experiment was performed as follows: the DOX-loaded nanocarriers were resuspended into PBS pH 7.4 (the physiological pH) and into acetate Buffer pH 5.3 (the pH of cancer cells) and incubated at 37 °C while shaken at 500 rpm. After predetermined time intervals, nanocarriers were separated from the buffer by centrifugation. The concentration of released DOX from each nanocarrier in the supernatant was measured by UV–Vis–NIR spectroscopy at the wavelength of 480 nm using a calibration curve prepared under the same condition. The percentage of drug released was obtained using the following equation:

$$\%\,DOX\ released = \frac{mass\ of\ released\ DOX}{mass\ of\ loaded\ DOX} \times 100 \tag{7}$$

2.7.1. Mechanism of DOX release

To examine the drug release mechanism of loaded DOX from GO-Phe-CD-DOX, four model, including Zero order (Eq. (8)), First order (Eq. (9)), Higuchi (Eq. (10)), and Korsmeyer-Peppas (Eq. (11)) (Dash, Murthy, Nath, & Chowdhury, 2010), were used as follows to fit the accumulative release data.

$$Q_t = Q_0 + K_0 t \tag{8}$$

where Q_t is the amount of drug dissolved in time t, Q_0 is the initial amount of drug in the solution and K_0 is the zero order release constant expressed in units of concentration/time. To examine the release kinetics, data obtained from *in vitro* DOX release studies were plotted as cumulative amount of DOX released (%Q) *vs.* time.

$$LnC = LnC_0 - K_t/2.303 \tag{9}$$

where C_0 is the initial concentration of DOX, K is the first order rate constant, and t is the time. The data obtained are plotted as Ln(%Q) of DOX remaining *vs.* time.

$$Q = K_H \times t^{1/2} \tag{10}$$

where, K_H is the Higuchi dissolution constant. The data obtained were plotted as %Q DOX release *vs.* square root of time.

$$\frac{M_t}{M_\infty} = Kt^n \tag{11}$$

where, M_t/M_∞ is the fraction of DOX released at time t, K is the rate constant and n is the release exponent. The n value is used to characterize different release.

2.8. Cell toxicity studies

The *in vitro* cytotoxicity of prepared samples was studied on human breast cancer cells, MCF-7 cells (DOX-sensitive), by MTT and trypan blue dye exclusion assays.

2.8.1. MTT cytotoxicity assay

A cell count of 10^4 MCF-7 cell was seeded in 96-plates. After 24 h of incubation at 37 °C and 5% CO_2, the cells were treated with the culture medium containing various concentration (2–50 μg/mL) of GO, GO-Phe, GO-Phe-CD, free DOX, GO/DOX, GO-Phe/DOX, GO-Phe-CD/DOX to evaluate cytotoxicity of the prepared graphene based nanocarriers for 48 h. Then, the medium was replaced with 100 μL of MTT (0.5 mg/mL) in PBS and incubated for another 3 h. Finally, the medium was aspirated and the remaining formazan crystals were solubilized in 100 μL DMSO. Light absorbance was measured at 570 nm and corrected for the background absorbance at 650 nm. Cell viability was calculated as percentage relative to untreated control cells (Gerlier & Thomasset, 1986).

2.8.2. Trypan blue membrane integrity assay

MCF-7 cells were seeded (10^6 cells/well) in 6-well plates. After 24 h, the cells were incubated with various concentration (2–50 μg/mL) of GO, GO-Phe, GO-Phe-CD, free DOX, GO/DOX, GO-Phe/DOX, and GO-Phe-CD/DOX for 48 h. Next, the cells were trypsinized and suspended in PBS containing trypan blue dye and then counted to determine the percentage of viable cells (with clear cytoplasm) *versus* non-viable cells (blue stained cytoplasm) using hemocytometer. Cell membrane leakage (%) was expressed as the percentage of non-viable to the total cells. The untreated cells served as control (Strober, 2001).

2.9. Statistical analysis

Statistical analysis was performed by Prism Software version 6.0 (GraphPad, USA). The results are expressed as the mean vales ± standard deviation (SD) and analyzed using Student's t-test. Values of $P \leq 0.05$ is considered to be statistically significant.

3. Results and discussion

3.1. GO-Phe-CD nanocarrier preparation

To improve graphene stability in biological media and to enhance drug loading capacity and biocompatibility, β-CD was grafted onto graphene. To this aim, GO was first functionalized by Phe and then β-CD was grafted onto GO-Phe. The typical procedure for the preparation of the GO-Phe-CD nanocarrier is illustrated in Fig. 1. GO was synthesized through Hummers method and carboxylic acid, hydroxyl and epoxy groups were introduced onto the edge and basal plane of the graphene layers. In the next step, Phe was attached to GO *via* the

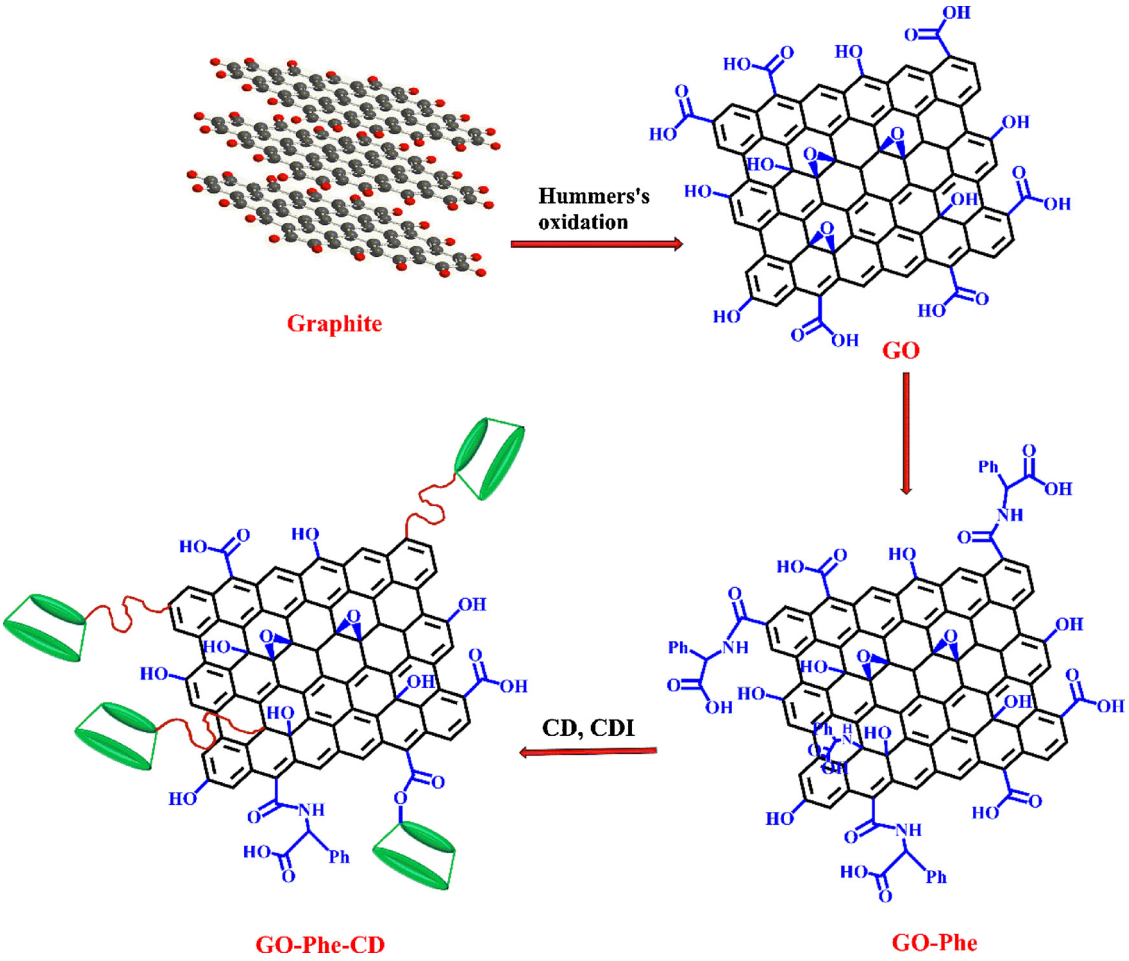

Fig. 1. Schematic illustration of GO-Phe-CD synthesis.

reaction of Phe NH_2 groups with carboxylic acid and epoxy functionalities on GO. Phe not only causes the improvement of GO solubility in biological media, but it also acts as a linker to create a distance between GO surface and β-CD moieties and might decrease the shielding effect of GO sheet. Finally, the free carboxylic acid groups, were activated by CDI and then β-CD was attached onto GO surface.

3.2. Characterization of GO-Phe-CD nanocarrier

3.2.1. Raman spectroscopy

Generally, graphene Raman spectrum contains three featured peaks at 1355 (D), 1575 (G) and ~ 3000 (2D) cm^{-1} (Fig. 2A(a)). The D band is the result of the defects and disordered structure which is weak in pure graphite. The G peak corresponds to the first order scattering of the E_{2g} phonon of the sp^2 carbon atoms, which is prominent in neat graphite (Ferrari, 2007; Wu, Lin, Cong, Liu, & Tan, 2018). As graphite was oxidized or functionalized, the position and intensity of these peaks will vary by revealing some useful aspects. As shown, after oxidation (Fig. 2A(b)), the intensity of D band is increased and the I_D/I_G ratio is much higher (0.90) than graphite (0.10), which reveals an increase in the degree of disorder due to introduction of oxygen containing groups onto the graphene basal plane, especially epoxide groups. When GO was functionalized by Phe, I_D/I_G ratio increased from 0.90 to 1.06 (Fig. 2A(c)), indicating that the attachment of amino acid moieties caused an increase in structural defects in GO and confirmed GO functionalization with Phe. Further GO functionalization by β-CD led to more enhancement of I_D/I_G ratio (1.26) (Fig. 2A(d)), which resulted in more edges and defects in the GO.

Moreover, in biological application, the lateral dimension of graphene nanomaterials is an important factor. Cell uptake, transport, biological degradation and toxicity of these nanomaterials depends on their dimensions. Consequently, size determination of graphite carbon cluster is important. In Raman spectroscopy, the I_D/I_G ratio is used to determine the size of sp^2 domains. The size of sp^2 carbon clusters of graphite, GO, GO-Phe and GO-Phe-CD nanocarriers was calculated using Knight's empirical formula (Eq. (12)) (Knight & White, 2011):

$$L_a = 4.35 \Big/ \left(I_D/I_G\right) \tag{12}$$

where L_a is the size of sp^2 carbon clusters and I_D/I_G is the intensity ratio of D and G bands. According to data in Table S1, it can be concluded that conjugation of GO with CD leads to a gradual reduction of graphitic structure causing an enhancement of I_D/I_G ratio as well as decreasing the size of the graphitic domains (Dong et al., 2012; Kundu, Nandi, Das, & Nandi, 2015).

Another important factor regarding graphene application as a drug carrier is the number of its layers. The surface area will decrease when the number of graphene layers increase. Furthermore, the rigidity of the graphene nanocarriers, which is highly relevant to cell penetration, will also increase by enhancing the number of layers. The shift in G band position and the 2D peak intensity, shape and position reveal good information about the number of graphene layers (Ferrari, 2007). In this study, the G band exhibits a gradual blue shift from 1575 cm^{-1} for graphite to 1602 cm^{-1} for GO-Phe-CD nanocarrier. The introduction of Phe and β-CD molecules, the removal of unstable oxygen functional groups and the decrease in the number of layers lead to G band blue shift. The 2D band also exhibits red shift which is due to the decrease of the graphene layer numbers, estimated to be about 2–6 layers (Kudin

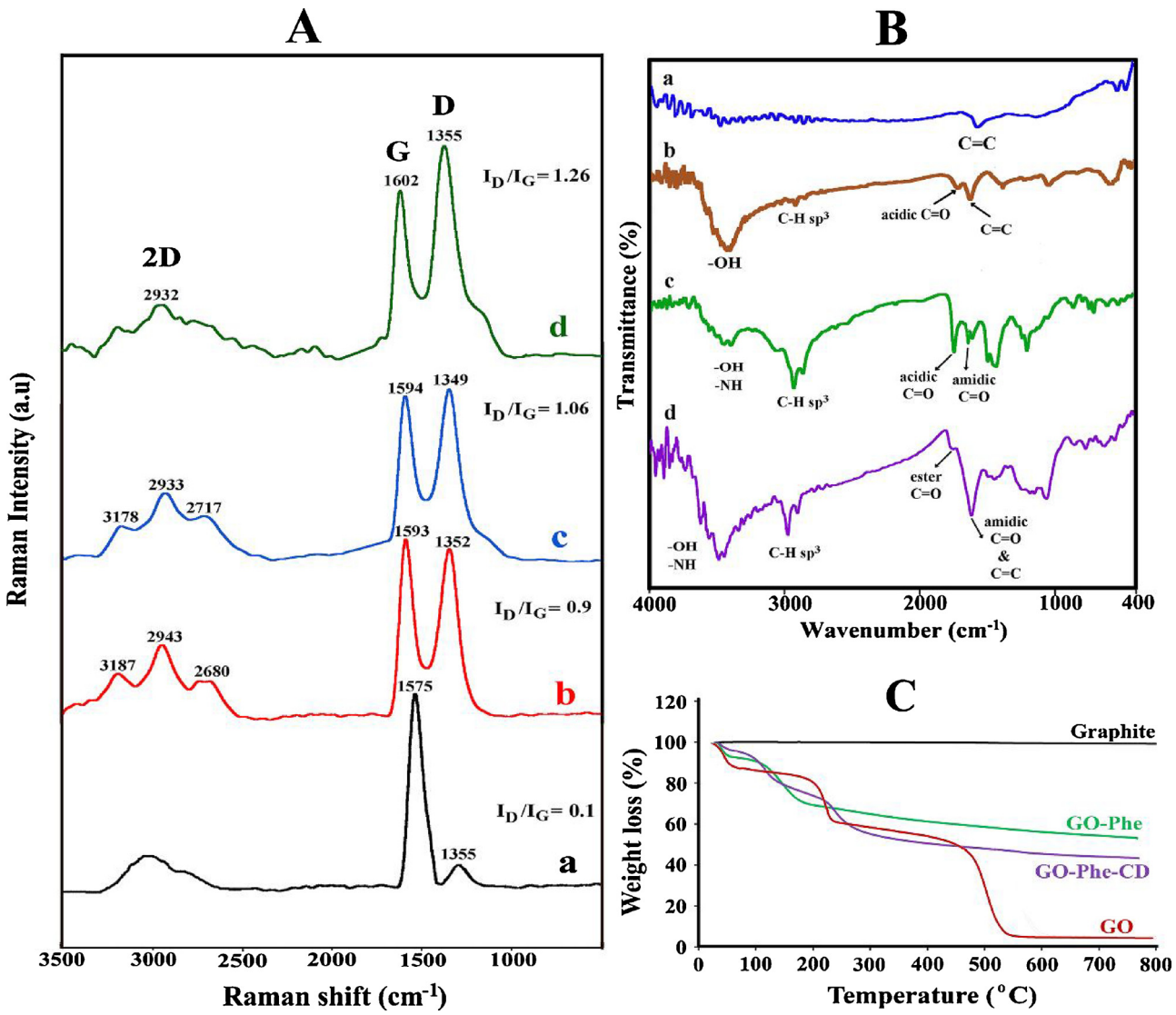

Fig. 2. (A) Raman spectra of (a) graphite; (b) GO; (c) GO-Phe; (d) GO-Phe-CD; (B) FT-IR spectra of (a) graphite; (b) GO; (c) GO-Phe; (d) GO-Phe-CD; (C) TGA curves of pure graphite; GO; GO-Phe and GO-Phe-CD with the heating rate of 10 °C/min.

et al., 2008).

3.2.2. FT-IR spectroscopy

Fig. 2B presents FT-IR spectra of graphite, GO, GO-Phe and GO-Phe-CD. The FT-IR spectrum of pure graphite (Fig. 3B(a)) does not show any featured peak except a peak at 1600 cm^{-1} which is assigned to C=C bonds. Compared to graphite spectrum, the presence of several peaks at GO FT-IR spectrum (Fig. 2B(b)), confirms the oxidation process. The peaks at 3430 cm^{-1}, 2922 cm^{-1} and 1719 cm^{-1} are attributed to the −OH stretching bands of hydroxyl and carboxylic acid groups, aliphatic sp^3 C–H stretching, and C=O stretching groups of carboxylic acids, respectively. For GO-Phe (Fig. 2B(c)), the appearance of carboxylic acid and amidic C=O stretching vibration at 1725 and 1640 cm^{-1}, confirms GO functionalization by Phe (Mallakpour et al., 2014). In the GO-Phe-CD spectrum (Fig. 2B(d)), new peak at 1730 cm^{-1} is assigned to ester C=O band, which confirms covalent attachment of β-CD onto GO-Phe surface.

3.2.3. Thermal analysis

Fig. 2C displays TGA curves of pure graphite, GO, GO-Phe and GO-Phe-CD conjugate. Graphite shows no weight loss until 800 °C. In GO TGA curve, three weight loss steps are observed. The first stage, which occurs below 100 °C, is assigned to the volatilization of adsorbed water on GO structure. The second weight loss at 200–250 °C is attributed to the pyrolysis of labile oxygen-containing groups, such as hydroxyl, epoxy and carboxyl groups. The last stage begins around 500 °C is related to the GO skeleton breakdown (Kuilla et al., 2010; Mallakpour et al., 2014). The weight loss at 150–250 °C in TGA curve of GO-Phe and GO-Phe-CD is assigned to the pyrolysis of the attached amino acid molecules and it is also found that the weight loss region at 230–350 °C for GO-Phe-CD could be attributed to the decomposition of β-CDs. So, the amount of β-CD molecules was determined to be 25 wt%.

3.2.4. FE-SEM and TEM analysis

The FE-SEM images of GO and GO-Phe-CD are shown in Fig. 3a and b, respectively. In contrast to GO, the FE-SEM images of GO-Phe-CD exhibits more uneven surface topology, lower transparency and higher layer thickness, which can be due to β-CD grafting on the GO-Phe-CD surfaces. According to the FE-SEM images, a uniform surface morphology and topology can be seen for both GO and GO-Phe-CD, which reveal that the oxidation and functionalization method would not damage the layered structure of GO.

In addition, from the TEM images of GO-Phe-CD (Fig. 3c), the layer structure and wrinkled sheets of GO and block morphology of β-CD can

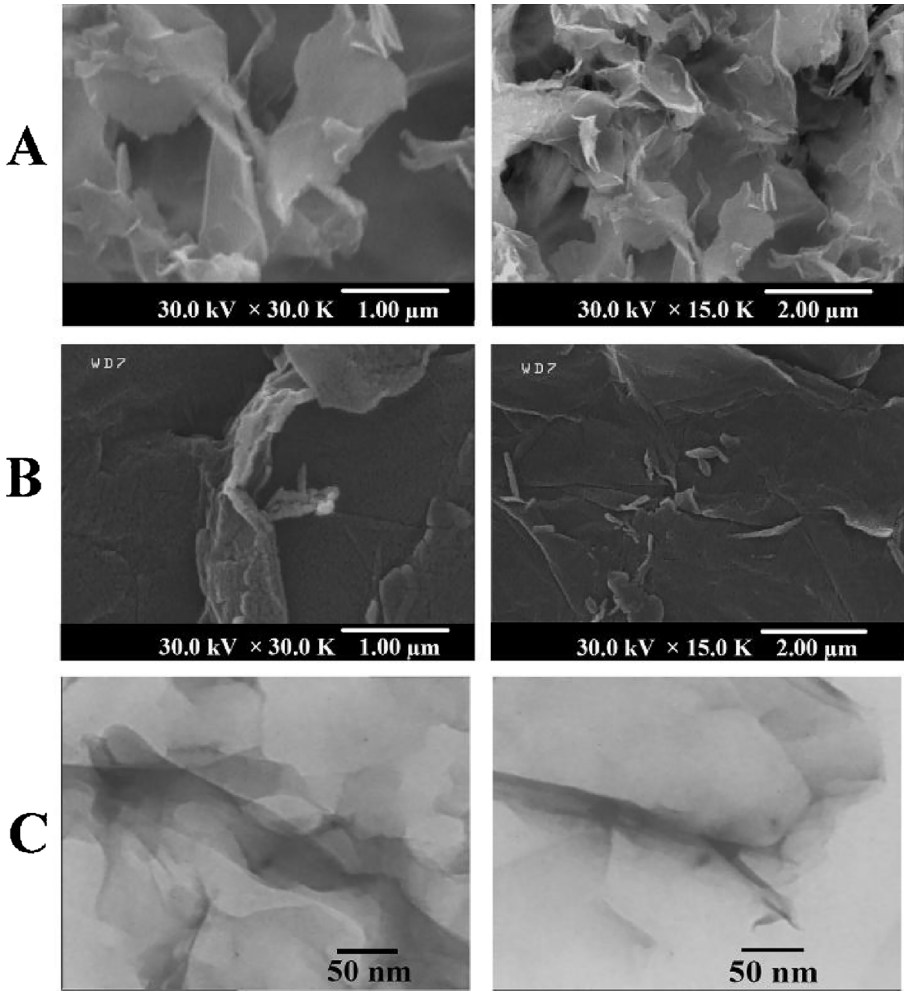

Fig. 3. FE-SEM images of (A) GO; (B) GO-Phe-CD at different magnifications; (C) TEM images of GO-Phe-CD.

be seen. These results confirm that β-CD molecules have been attached onto the surface of GO.

3.2.5. Particle size distribution and ζ potential

The hydrodynamic diameters of GO, GO-Phe and GO-Phe-CD in D.I. water as determined by DLS are listed in Table S2. The mean size of GO sheets was 312 ± 4.2 nm and after CD grafting the thickness of GO-Phe-CD nanocarrier increased significantly and the mean size determined by DLS was increased to 520 ± 0.89 nm. This size changing confirms successful CD attachment onto the GO surface.

In addition, for *in vitro* cytotoxicity investigations, the surface charge and aggregation state of nanomaterials are critically important in cell-nanoparticle interactions. In most cases, for cytotoxicity study of nanomaterials, the particles are suspended in balanced salt solution, like phosphate buffered saline (PBS). Therefore, in this study, besides D.I. water, the colloidal stability of prepared nanocarriers was also evaluated in PBS, since the findings are perfectly similar to their actual particulate state in toxicity assays and biological environments. According to Table S2, the zeta (ζ)-potentials of all graphene based nanocarriers are negative. Compared to GO, GO-Phe and GO-Phe-CD have higher ζ-potential, which is consistent with amino acid functionalization and β-CD grafting and the increased oxygen amount onto the surface of GO, especially in the case of β-CD conjugation. Due to the electrostatic repulsion of colloidal particles, solutions with ζ-potential greater than −30 mV are considered as stable. Hence, when the absolute value of the ζ-potential increase, it is suggested that the dispersion stability will rise (Hayyan, Abo-Hamad, AlSaadi, & Hashim, 2015; Kashyap, Mishra, & Behera, 2014). Herein, the absolute value of GO-Phe-CD ζ-potential is higher than the others, which reveals its more dispersion stability compared to GO and GO-Phe. Higher dispersion stability is very useful for *in vitro* cytotoxicity assay. Furthermore, the ζ-potentials of all samples are lower in PBS compared to D.I. water. This is due to charge neutralization of surface oxygen groups by ionic salt species. Moreover, of the GO-Phe-CD-DOX was more electropositive than GO-Phe-CD (Table S2). The positively charged DOX could electrostatically bind with the negative nanocarrier, making the net charge more electropositive than that of the GO-Phe-CD only. The changes of ζ-potential values revealed that DOX was successfully loaded onto the GO-Phe-CD nanocomposite.

3.3. DOX loading onto GO based nanocarriers

DOX, an anti-tumor model drug, was loaded onto the surface of GO, GO-Phe and GO-Phe-CD *via* a simple mixture and sonication method. The unbound drug was removed by centrifugation and the loading capacity and efficiency of DOX on GO-based nanocarriers were calculated by measuring the concentration of unbound drug using UV–vis spectra and the data are presented in Table 1. According to the data, the loading efficiency and loading capacity of GO-Phe-CD are higher than the others, and are as high as 78.7% and 85.2%, respectively, when the solution of DOX with an initial concentration at 1 mg/mL was used. The interaction between GO, GO-Phe and GO-Phe-CD with DOX can be due to π-π staking between the conjugated structure of graphene sheet and the quinone portion of DOX, and the hydrophobic effect between them.

Table 1
The results of DOX loading on GO, GO-Phe and GO-Phe-CD.

Nanocarrier	%LC	%LE
GO	46.0	42.5
GO-Phe	48.0	44.4
GO-Phe-CD	85.2	78.7

Moreover, the hydrogen bonding between the −OH, −NH and −COOH groups of nanocarriers and DOX −OH and -NH_2 groups is possible, which was reported in the literature (Yang et al., 2008). In the case of GO-Phe-CD, the DOX loading efficiency and loading capacity are nearly twice higher than the corresponding value of GO and GO-Phe, which can be due to the encapsulation of β-CD cavity towards anti-cancer drug. Complexation ability of β-CD is very useful to enhance drug loading (Gidwani & Vyas, 2015; Shelley & Babu, 2018). Fig. 4 depicts possible interactions between DOX and GO-Phe-CD, including π-π staking, hydrogen bonding and complexation interactions. As shown, the cone shaped cavity of CD act as a host for loading of hydrophobic DOX (guest) through van der Waals interaction, hydrogen bonds and formation of host–guest inclusion complex.

3.3.1. Adsorption kinetic models

To examine the kinetic adsorption of DOX on the GO-Phe-CD nanocarrier, different kinetic models, such as Langmuir, Freundlich, Dubinin-Radushkevich and Temkin were used, and the obtained results are presented in Fig. 5. In addition, the corresponding kinetic parameters are summarized in Table 2. Correlation coefficient (R^2) was used to evaluate the validity of each kinetic model. By comparing the obtained R^2 values, the Langmuir adsorption model was found to be more applicable for DOX adsorption on GO-Phe-CD. DOX adsorption data on GO-Phe-CD fits well with the Langmuir isotherm model with higher R^2 (0.9774). The fitness of the adsorption data to the Langmuir isotherm indicates that the adsorption of DOX on GO-Phe-CD is a monolayer adsorption (Patiha, Heraldy, Hidayat, & Firdaus, 2016) and might be due to the homogeneous distribution of active sites on the edge and two sides of the GO-Phe-CD sheet, since the Langmuir equation assumes that the surface is homogeneous (Wu et al., 2013). In addition, the maximum adsorption capacity (Q_m) of GO-Phe-CD for DOX is 1204 mg/g through curve fitting of Langmuir isotherm adsorption, which is higher than those of reported carriers for DOX adsorption (Cao, Yue, Li, & Dai, 2013; Wang et al., 2015).

3.4. pH stimuli-responsive release of DOX

The extracellular pH in normal tissues and blood is approximately 7.4 whereas in extracellular tumor tissues, the average pH is drastically acidic (pH 4.5 − 6.5). Hence, to enhance the release of anti-cancer drug inside the tumor tissue or cells and to avoid undesired release during the delivery process in blood circulation, it is necessary that drug release from the nanocarrier to be pH-responsive. Therefore, it is necessary to investigate controlled drug release from the DOX-loaded graphene based nanocarriers at 37 °C. In addition, due to high loading capacity of GO-Phe-CD toward DOX, it can be used as a drug carrier candidate material. Thus, the release behavior of DOX from GO-Phe-CD at two different pH conditions (pH 5.3 and 7.4) and various times was

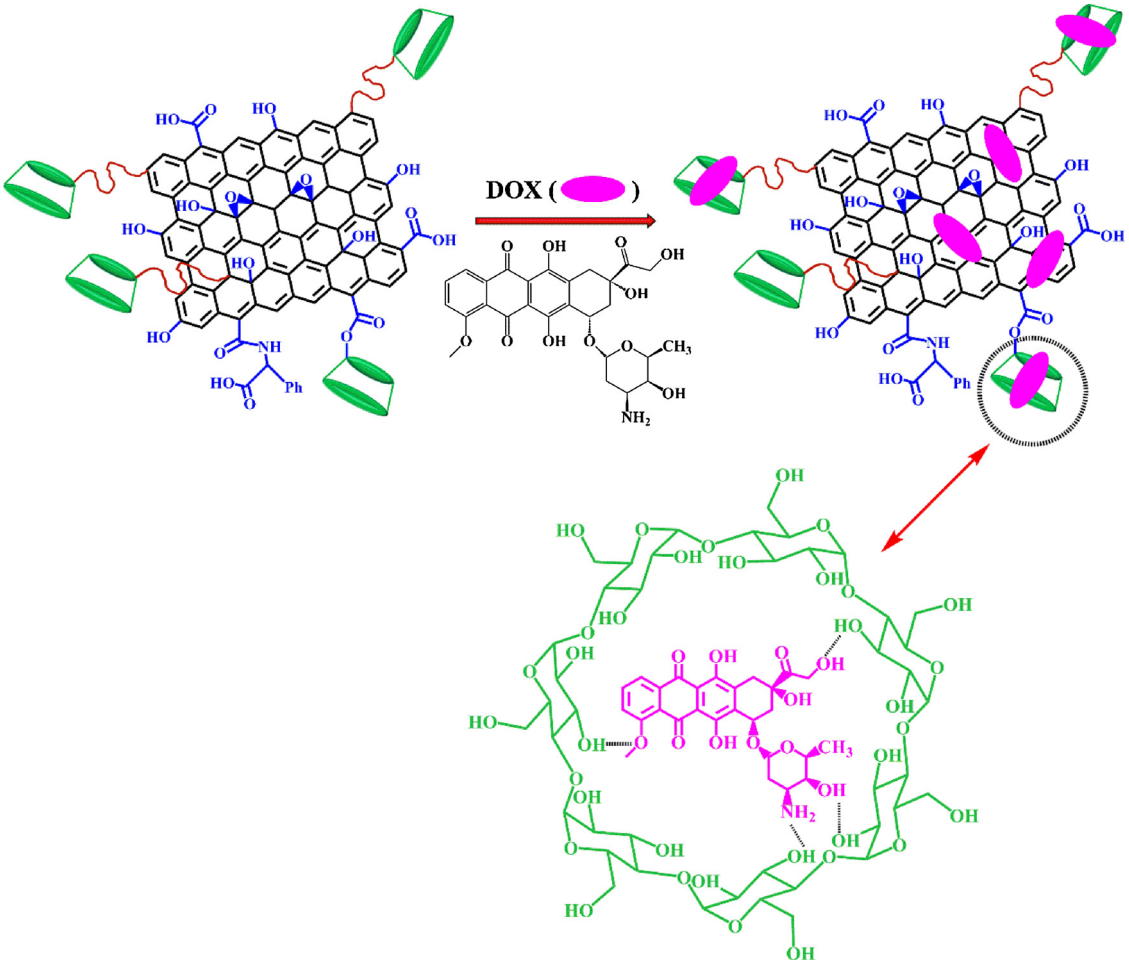

Fig. 4. The possible interactions between DOX and GO-Phe-CD nanocarrier.

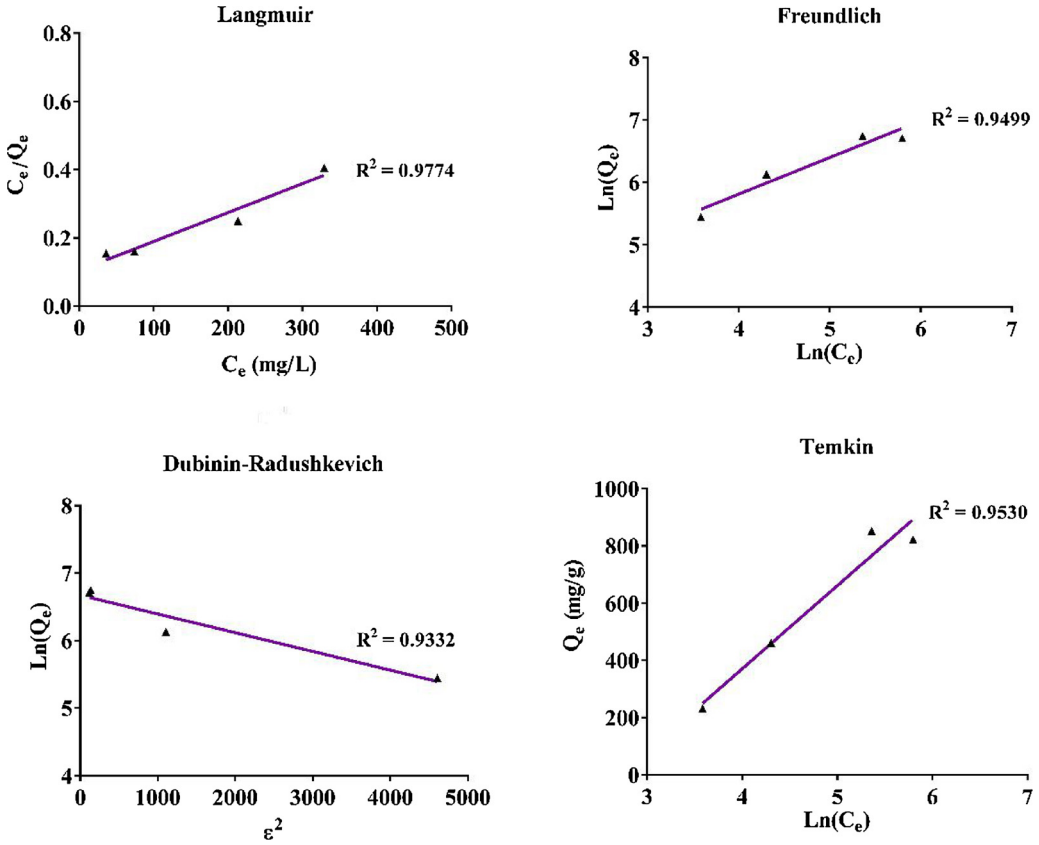

Fig. 5. The Langmuir, Freundlich, Dubinin-Radushkevich and Temkin Isotherms for DOX adsorption on GO-Phe-CD nanocarrier.

examined and is shown in Fig. 6A.

As seen in Fig. 6A, at normal physiological condition (pH 7.4), the DOX is released from GO-Phe-CD nanocarrier slowly and only 12% of the total bound DOX is released after 72 h, which can be due to the existence of strong hydrogen bonding interactions between DOX and nanocarrier leading to a slow and inefficient release. In acidic condition (pH 5.3), the release ratio of DOX was dramatically enhanced with 40% of DOX released in 72 h, which can be due to desorption of bounded DOX molecules on GO-Phe-CD surface in effect of protonation of DOX amine groups and hydrogen bonding breakage between DOX and the GO-Phe-CD nanocarrier, leading to a higher preferred release of DOX. Furthermore, another reason can be due to the release of entrapped DOX molecules in β-CD cavities in acidic pH. Apart from the GO surface chemistry, apparent drug solubility at certain pH should be considered as a driving force for drug release. Considering pK_a of DOX amine (~ 8.2), the drug solubility would be more favorable at more acidic pH than 7.4 due to protonation of the amine group. It was also revealed that the GO-Phe-CD nanocarrier ζ-potential decreases following the drug loading (Table S2), confirming surface association of the protonable drug (DOX) on GO-Phe-CD. This effect was clearly more pronounced at pH = 7.4 than 5.3 that could be explained by abrupt surface dissociation or release of DOX at acidic pH of 5.3. As shown in Fig. 6A, even at pH 5.3, complete release of DOX did not occur, which can be as a result of diffusion equilibrium between GO-Phe-CD and drug inclusion complexes.

3.4.1. DOX release mechanism

To investigate DOX release mechanism from GO-Phe-CD-DOX, first 60% accumulative drug release data at pH 7.4 and 5.3 were fitted in Zero order, First order, Higuchi, and Korsmeyer-Peppas models and are shown in Fig. 6B. The obtained release parameters are also listed in Table 3. The best-fit model was determined by R^2. According to different models' R^2, the Higuchi release model was much desired (0.9146 and 0.9831 for pH 7.4 and 5.3), which suggests simple diffusion DOX release.

In addition, the n value of Korsmeyer-Peppas model can be used to characterize the release mechanism of DOX. In this model, $0.45 \leq n$ corresponds to a Fickian diffusion mechanism, $0.45 < n < 0.89$ to anomalous (non-Fickian) diffusion, $n = 0.89$ to Case II transport, and $n > 0.89$ to super case II transport (Ritger & Peppas, 1987; Siepmann & Peppas, 2001). Accordingly, the DOX mechanism release at pH 7.4 is the Fickian diffusion mechanism (n = 0.4271) and at pH 5.3 is the anomalous (non-Fickian) diffusion (0.6423).

3.5. In vitro cytotoxicity of GO based nanocarriers

To evaluate the potential application of prepared GO based nanocarriers in the biomedical field, the cytotoxicity of GO, GO-Phe and GO-

Table 2
Isotherm parameters for the adsorption of DOX on GO-Phe-CD.

Langmuir			Freundlich			Dubinin-Radushkevich			Temkin		
Q_m (mg/g)	K_L (L/g)	R^2	K_F (L/g)	n	R^2	Q_s (mg/g)	K_D (mol^2/kJ^2)	R^2	K_T (L/g)	b	R^2
1204	0.0083	0.9774	54.37	2.06	0.9499	788.39	0.00027	0.9332	15.18	8.54	0.9530

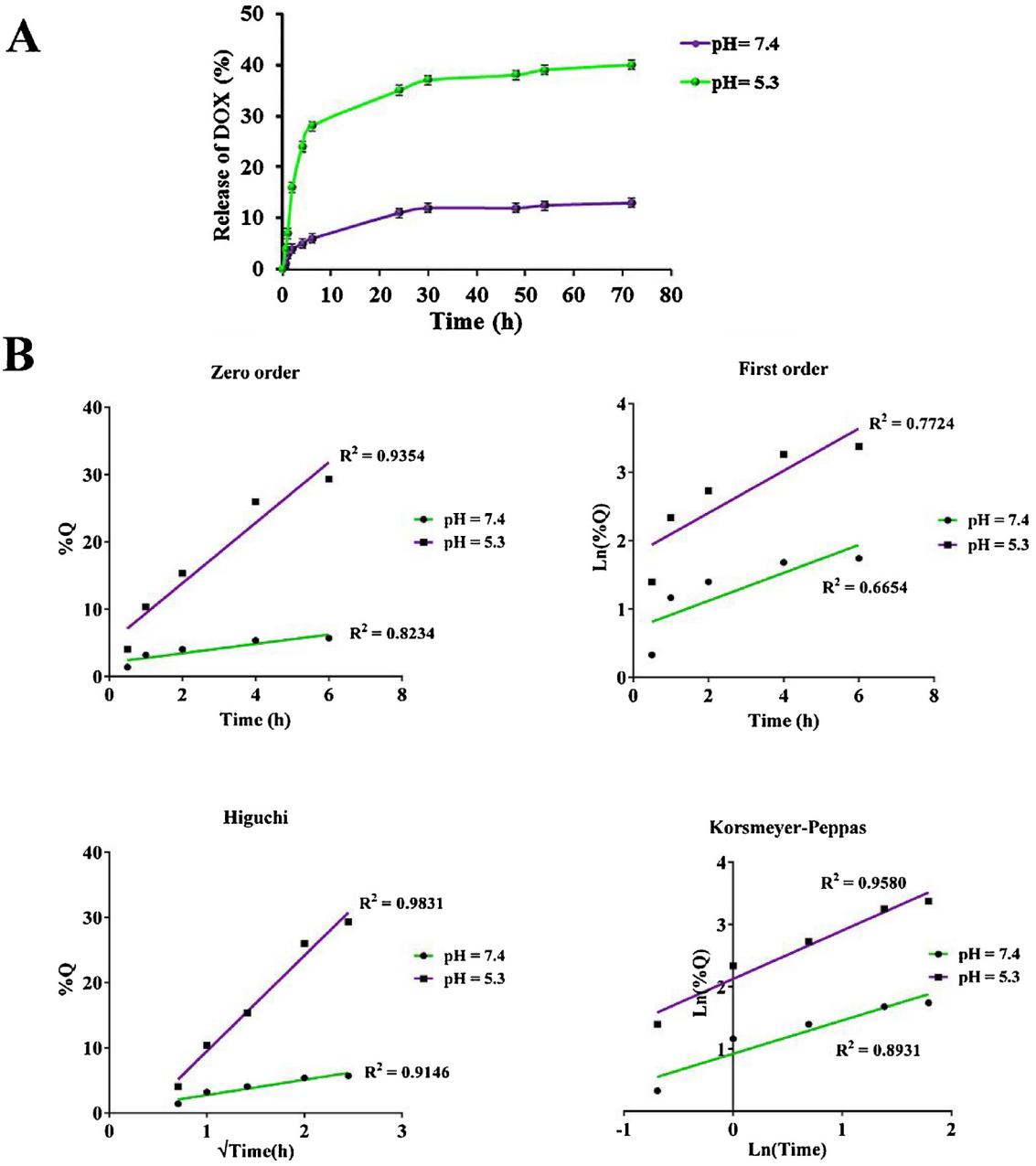

Fig. 6. (A) DOX release from GO-Phe-CD nanocarrier at pH 7.4 and 5.3 by UV − vis analysis at 480 nm at room temperature. Each value represents the mean ± SD (n = 3); (B) The curves of the Zero-order, First-order, Higuchi and Korsmeyer-Peppas equation models of drug release from the DOX-loaded GO-Phe-CD.

Table 3
Release parameters of DOX from GO-Phe-CD at pH 7.4 and pH 5.3 obtained from four kinds of kinetic models.

pH	Zero-order		First-order		Higuchi		Korsmeyer-Peppas	
	K_0	R^2	Q_{inf}	R^2	K_h	R^2	n	R^2
7.4	1.18	0.8234	5.77	0.6654	2.57	0.9146	0.4271	0.8931
5.3	5.63	0.9354	35.27	0.7724	11.75	0.9831	0.6423	0.9580

Phe-CD nanocarriers and its cell killing capability with these pH responsive DOX-loaded drug delivery systems were examined. To this aim, two assay methods, the MTT assay and trypan blue exclusion, were employed for MCF-7 cell lines and the obtained results were compared. Fig. 7A presents cell viability of MCF-7 cells determined from MTT assay after 48 h of exposure to different concentrations of various GO based nanocarriers, either empty or DOX loaded. Fig. 7B displays cell viability of MCF-7 cells determined from trypan blue exclusion after 48 h exposure to different concentration of various GO based nanocarriers, free DOX and DOX loaded nanocarriers. According to the MTT assay results (Fig. 7A(a)), no dose-dependent effects on the mitochondrial activity of MCF-7 cells was seen for different nanocarriers. In addition, there was no significant difference between cytotoxicity of various nanocarriers, which did not show the effect of functionalization on the GO cytotoxicity. These observations, reveal that the cells were unaffected by either nanocarriers at any concentration. Furthermore, after DOX loading (Fig. 7A(b)), the cell viability was still high and the ability of DOX-loaded nanocarriers for killing MCF-7 cells was not determined by MTT assay. These findings conformed the previous study by Liao et al. (Liao, Lin, Macosko, & Haynes, 2011). According to their results, the MTT assay was not suitable for the investigation of graphene derivatives' cytotoxicity. It was mentioned that graphene derivatives lead to a false positive measure of viability, causing an

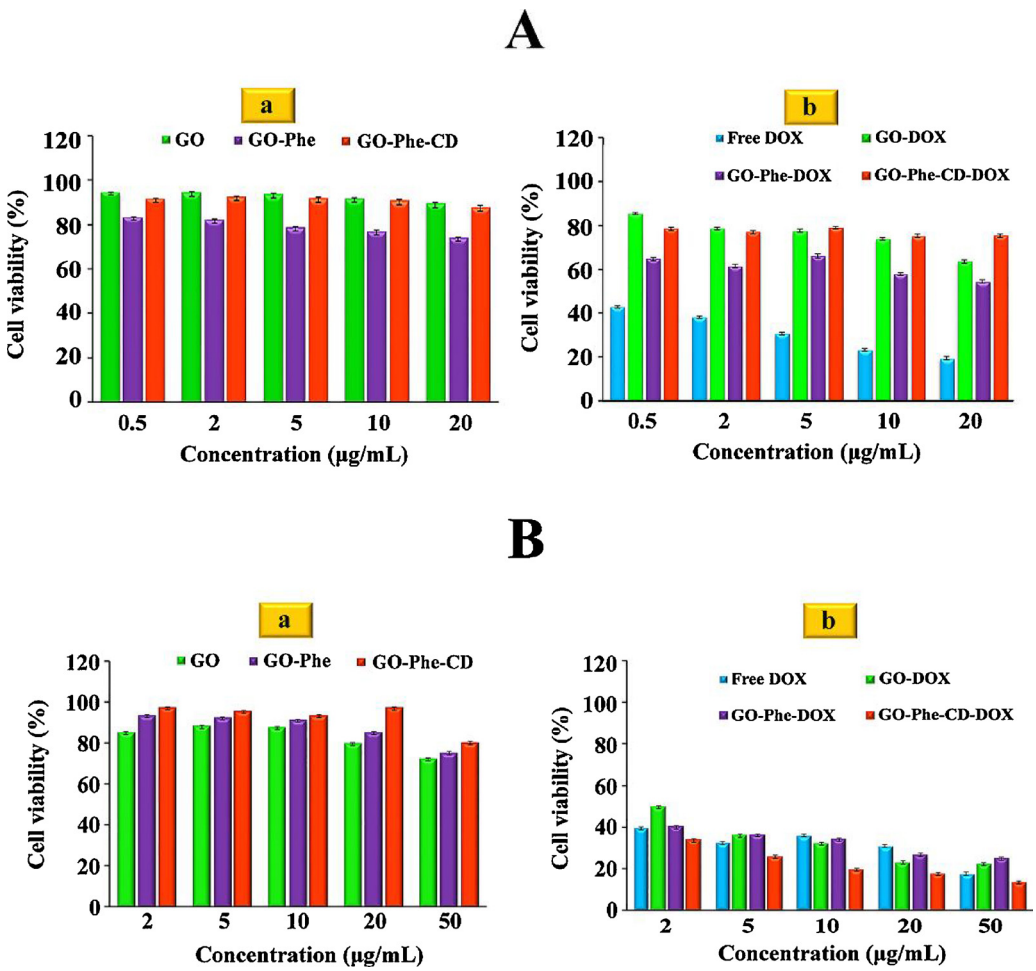

Fig. 7. (A) Cell viability of MCF-7 cells determined from MTT assay after 48 h exposure to different concentration of (a) various GO based nanocarriers and (b) DOX loaded nanocarriers; (B) Cell viability of MCF-7 cells determined from trypan blue exclusion after 48 h exposure to different concentration of (a) various GO based nanocarriers and (b) free DOX and DOX loaded nanocarriers. Data represent mean ± SD (n = 3).

overestimation of the human skin fibroblast viability. Monteiro-Riviere et al. (Monteiro-Riviere & Inman, 2006) and Wörle-Knirsch et al. (Wörle-Knirsch, Pulskamp, & Krug, 2006) also reported the interference of carbon-based materials with MTT reagent, generating overestimated viability results. Moreover, Marques et al. (Marques et al., 1995) reported that the $[MTT]^+$ cation can be reduced by GO electrons and protons with a detailed reaction mechanism. Therefore, the MTT assay is not an appropriate technique for predicting the cytotoxicity of graphene based materials due to the spontaneous formation of MTT formazan by these materials leading to a false high biocompatibility.

In contrast to the MTT assay results, trypan blue dye exclusion data (Fig. 7B) demonstrate a dose-dependent effect on the viability of MCF-7 cells. As shown in Fig. 7B(a), GO-Phe-CD possess lower toxicity on MCF-7 cells in the given concentration range, in comparison with the other nanocarriers. The superior cytocompatibility of the GO-Phe-CD nanocarrier compared to the other GO based nanocarriers can be explained by its absolute value of zeta potential (Table S2) due to conjugation of biocompatible β-CD molecules onto graphene surface.

In addition, the therapeutic efficiency of the DOX-loaded nanocarriers and free DOX in MCF-7 cells were also performed and the obtained results are presented in Fig. 7B(b). Free DOX alone greatly reduced the viability of MCF-7, especially at 50 μg/mL concentration. However, the cell-killing activity of DOX-loaded GO-Phe-CD nanocarrier was much higher than the others. Compared to the pure nanocarrier, the higher cytotoxicity of DOX-loaded GO-Phe-CD at similar concentration, confirmed that the GO-Phe-CD had significant cytocompatibility, and the DOX-loaded GO-Phe-CD had outstanding killing capability to MCF-7 cells.

4. Conclusion

In conclusion, in this study, a high anti-cancer drug loading and pH-responsive GO-Phe-CD nanocarrier was developed, which exhibited excellent water and PBS dispersity and stability. DOX can easily be loaded into the GO-Phe-CD with high loading efficiency and capacity (1204 mg/g). The *in vitro* release of DOX was higher in acidic milieu of cancer cells compared to physiological conditions. These results were the outcome from the host–guest inclusion complex between CD and DOX, leading to enhance DOX loading and its control release. The comparison between the two techniques for cytotoxicity measurement (MTT assay and trypan blue dye exclusion) revealed that the MTT assay was not an appropriate technique for predicting the cytotoxicity of graphene based materials due to the spontaneous formation of MTT formazan by these materials leading to a false high biocompatibility. More significantly, the cytotoxicity investigation showed that the GO-Phe-CD nanocarrier had no noticeable toxicity on MCF-7 cells, while the DOX-loaded GO-Phe-CD had outstanding killing capability. Consequently, GO-Phe-CD nanocarrier possesses excellent biocompatibility, and is a pH-responsive drug delivery system, which can be a suitable candidate for delivery of chemotherapeutic drugs such as DOX.

Acknowledgment

This study was funded by a grantfrom Shiraz University of Medical

Sciences (SUMS), Deputy of Research and Technology, research project no. 95-01-81-13006. The authors also gratefully acknowledge use of the facilities of the Center for Nanotechnology in Drug Delivery at SUMS. The authors thank Samaneh Mohammadi for technical assistance. The authors wish to thank Mr. H. Argasi at the Research Consultation Center (RCC) of SUMS for his invaluable assistance in editing this manuscript.

Appendix A. Supplementary data

Supplementary material related to this article can be found, in the online version, at doi:https://doi.org/10.1016/j.carbpol.2018.08.064.

References

Abdolmaleki, A., Mallakpour, S., & Borandeh, S. (2015). Efficient heavy metal ion removal by triazinyl-β–cyclodextrin functionalized iron nanoparticles. *RSC Advances, 5*, 90602–90608.
Ayawei, N., Ebelegi, A. N., & Wankasi, D. (2017). Modelling and interpretation of adsorption isotherms. *Journal of Chemistry, 2017*, 11.
Cao, Z., Yue, X., Li, X., & Dai, Z. (2013). Stabilized magnetic cerasomes for drug delivery. *Langmuir, 29*(48), 14976–14983.
Chen, M., Diao, G., & Zhang, E. (2006). Study of inclusion complex of β-cyclodextrin and nitrobenzene. *Chemosphere, 63*(3), 522–529.
Dash, S., Murthy, P. N., Nath, L., & Chowdhury, P. (2010). Kinetic modeling on drug release from controlled drug delivery systems. *Acta Poloniae Pharmaceutica, 67*(3), 217–223.
Deb, A., & Vimala, R. (2018). Camptothecin loaded graphene oxide nanoparticle functionalized with polyethylene glycol and folic acid for anticancer drug delivery. *Journal of Drug Delivery Science and Technology, 43*, 333–342.
Dong, H., Li, Y., Yu, J., Song, Y., Cai, X., Liu, J., et al. (2012). A versatile multicomponent assembly via β-cyclodextrin host–guest chemistry on graphene for biomedical applications. *Small, 9*(3), 446–456.
Duran, N., Martinez, D. S., Silveira, C. P., Duran, M., de Moraes, A. C., Simoes, M. B., et al. (2015). Graphene oxide: A carrier for pharmaceuticals and a scaffold for cell interactions. *Current Topics in Medicinal Chemistry, 15*(4), 309–327.
Einafshar, E., Asl, A. H., Nia, A. H., Mohammadi, M., Malekzadeh, A., & Ramezani, M. (2018). New cyclodextrin-based nanocarriers for drug delivery and phototherapy using an irinotecan metabolite. *Carbohydrate Polymers, 194*, 103–110.
Farvadi, F., Tamaddon, A., Sobhani, Z., & Abolmaali, S. S. (2017). Polyionic complex of single-walled carbon nanotubes and PEG-grafted-hyperbranched polyethyleneimine (PEG-PEI-SWNT) for an improved doxorubicin loading and delivery: Development and in vitro characterization. *Artificial Cells, Nanomedicine, and Biotechnology, 45*(5), 855–863.
Feng, L., & Liu, Z. (2011). Graphene in biomedicine: Opportunities and challenges. *Nanomedicine (London, England), 6*(2), 317–324.
Ferrari, A. C. (2007). Raman spectroscopy of graphene and graphite: Disorder, electron–Phonon coupling, doping and nonadiabatic effects. *Solid State Communications, 143*(1), 47–57.
Gerlier, D., & Thomasset, N. (1986). Use of MTT colorimetric assay to measure cell activation. *Journal of Immunological Methods, 94*(1-2), 57–63.
Gidwani, B., & Vyas, A. (2015). A comprehensive review on cyclodextrin-based carriers for delivery of chemotherapeutic cytotoxic anticancer drugs. *BioMed Research International, 2015*, 15.
Golkar, N., Samani, S. M., & Tamaddon, A. M. (2016). Modulated cellular delivery of anti-VEGF siRNA (bevasiranib) by incorporating supramolecular assemblies of hydrophobically modified polyamidoamine dendrimer in stealth liposomes. *International Journal of Pharmaceutics, 510*(1), 30–41.
Hayyan, M., Abo-Hamad, A., AlSaadi, M. A., & Hashim, M. A. (2015). Functionalization of graphene using deep eutectic solvents. *Nanoscale Research Letters, 10*(1), 324.
Hong, B. J., Compton, O. C., An, Z., Eryazici, I., & Nguyen, S. T. (2012). Successful stabilization of graphene oxide in electrolyte solutions: Enhancement of biofunctionalization and cellular uptake. *ACS Nano, 6*(1), 63–73.
Hu, H., Yu, J., Li, Y., Zhao, J., & Dong, H. (2011). Engineering of a novel pluronic F127/graphene nanohybrid for pH responsive drug delivery. *Journal of Biomedical Materials Research Part A, 100A*(1), 141–148.
Hummers, W. S., & Offeman, R. E. (1958). Preparation of graphitic oxide. *Journal of the American Chemical Society, 80*(6) 1339-1339.
Karimi, Z., Abbasi, S., Shokrollahi, H., Yousefi, G., Fahham, M., Karimi, L., et al. (2017). Pegylated and amphiphilic Chitosan coated manganese ferrite nanoparticles for pH-sensitive delivery of methotrexate: Synthesis and characterization. *Materials Science and Engineering C, 71*, 504–511.
Kashyap, S., Mishra, S., & Behera, S. K. (2014). Aqueous colloidal stability of graphene oxide and chemically converted graphene. *Journal of Nanoparticles, 2014*, 6.
Kim, M.-G., Shon, Y., Miao, W., Lee, J., & Oh, Y.-K. (2016). Biodegradable graphene oxide and polyaptamer DNA hybrid hydrogels for implantable drug delivery. *Carbon, 105*, 14–22.
Knight, D. S., & White, W. B. (2011). Characterization of diamond films by Raman spectroscopy. *Journal of Materials Research, 4*(2), 385–393.
Kudin, K. N., Ozbas, B., Schniepp, H. C., Prud'homme, R. K., Aksay, I. A., & Car, R. (2008). Raman Spectra of graphite oxide and functionalized graphene sheets. *Nano Letters, 8*(1), 36–41.
Kuilla, T., Bhadra, S., Yao, D., Kim, N. H., Bose, S., & Lee, J. H. (2010). Recent advances in graphene based polymer composites. *Progress in Polymer Science, 35*(11), 1350–1375.
Kumar, R. V., Myeon-Cheon, C., Jin-Yeon, K., Yeon, K. G., Ju, K. M., Sun-Hee, K., et al. (2011). Synthesis and drug-delivery behavior of chitosan-functionalized graphene oxide hybrid nanosheets. *Macromolecular Materials and Engineering, 296*(2), 131–140.
Kundu, A., Nandi, S., Das, P., & Nandi, A. K. (2015). Fluorescent graphene oxide via polymer grafting: An efficient nanocarrier for both hydrophilic and hydrophobic drugs. *ACS Applied Materials & Interfaces, 7*(6), 3512–3523.
Liao, K.-H., Lin, Y.-S., Macosko, C. W., & Haynes, C. L. (2011). Cytotoxicity of graphene oxide and graphene in human erythrocytes and skin fibroblasts. *ACS Applied Materials & Interfaces, 3*(7), 2607–2615.
Liu, H., Liu, C., Yang, X., Zeng, S., Xiong, Y., & Xu, W. (2008). Uniformly sized β-cyclodextrin molecularly imprinted microspheres prepared by a novel surface imprinting technique for ursolic acid. *Analytica Chimica Acta, 628*(1), 87–94.
Liu, Z., Robinson, J. T., Sun, X., & Dai, H. (2008). PEGylated nanographene oxide for delivery of water-insoluble cancer drugs. *Journal of the American Chemical Society, 130*(33), 10876–10877.
Makharza, S., Cirillo, G., Bachmatiuk, A., Vittorio, O., Mendes, R. G., Oswald, S., et al. (2013). Size-dependent nanographene oxide as a platform for efficient carboplatin release. *Journal of Materials Chemistry B, 1*(44), 6107–6114.
Mallakpour, S., Abdolmaleki, A., & Borandeh, S. (2014). Covalently functionalized graphene sheets with biocompatible natural amino acids. *Applied Surface Science, 307*, 533–542.
Marques, E. P., Zhang, J., Tse, Y.-H., Metcalfe, R. A., Pietro, W. J., & Lever, A. B. P. (1995). Surface electrochemistry of 3-(4,5-dimethylthiazol-2-yl)-2,5-diphenyl-2H-tetrazolium bromide ([MTT]Br) adsorbed on a graphite electrode. *Journal of Electroanalytical Chemistry, 395*(1), 133–142.
Monteil, M., Lecouvey, M., Landy, D., Ruellan, S., & Mallard, I. (2017). Cyclodextrins: A promising drug delivery vehicle for bisphosphonate. *Carbohydrate Polymers, 156*, 285–293.
Monteiro-Riviere, N. A., & Inman, A. O. (2006). Challenges for assessing carbon nanomaterial toxicity to the skin. *Carbon, 44*(6), 1070–1078.
Muthoosamy, K., Bai, R. G., & Manickam, S. (2014). Graphene and graphene oxide as a docking station for modern drug delivery system. *Current Drug Delivery, 11*(6), 701–718.
Patiha, Heraldy, E., Hidayat, Y., & Firdaus, M. (2016). The langmuir isotherm adsorption equation: The monolayer approach. *IOP Conference Series: Materials Science and Engineering, 107*(1), 012067.
Ritger, P. L., & Peppas, N. A. (1987). A simple equation for description of solute release II. Fickian and anomalous release from swellable devices. *Journal of Controlled Release, 5*(1), 37–42.
Shelley, H., & Babu, R. J. (2018). Role of cyclodextrins in nanoparticle-based drug delivery systems. *Journal of Pharmaceutical Sciences, 107*(7), 1741–1753.
Siepmann, J., & Peppas, N. A. (2001). Modeling of drug release from delivery systems based on hydroxypropyl methylcellulose (HPMC). *Advanced Drug Delivery Reviews, 48*(2), 139–157.
Strober, W. (2001). Trypan blue exclusion test of cell viability. *Current Protocols in Immunology* Appendix 3, Appendix 3B.
Vogt, F. G., & Strohmeier, M. (2012). 2D solid-state NMR analysis of inclusion in drug–cyclodextrin complexes. *Molecular Pharmaceutics, 9*(11), 3357–3374.
Wakaskar, R. R. (2018). General overview of lipid–polymer hybrid nanoparticles, dendrimers, micelles, liposomes, spongosomes and cubosomes. *Journal of Drug Targeting, 26*(4), 311–318.
Wang, C., Li, B., Niu, W., Hong, S., Saif, B., Wang, S., et al. (2015). β-Cyclodextrin modified graphene oxide–magnetic nanocomposite for targeted delivery and pH-sensitive release of stereoisomeric anti-cancer drugs. *RSC Advances, 5*(108), 89299–89308.
Wang, C., Ravi, S., Garapati, U. S., Das, M., Howell, M., Mallela, J., et al. (2013). Multifunctional chitosan magnetic-graphene (CMG) nanoparticles: A theranostic platform for tumor-targeted co-delivery of drugs, genes and MRI contrast agents. *Journal of Materials Chemistry B, 1*(35), 4396–4405.
Wojtoniszak, M., Urbas, K., Perużyńska, M., Kurzawski, M., Droździk, M., & Mijowska, E. (2013). Covalent conjugation of graphene oxide with methotrexate and its antitumor activity. *Chemical Physics Letters, 568-569*, 151–156.
Wörle-Knirsch, J. M., Pulskamp, K., & Krug, H. F. (2006). Oops they did it again! carbon nanotubes hoax scientists in viability assays. *Nano Letters, 6*(6), 1261–1268.
Wu, J.-B., Lin, M.-L., Cong, X., Liu, H.-N., & Tan, P.-H. (2018). Raman spectroscopy of graphene-based materials and its applications in related devices. *Chemical Society Reviews, 47*(5), 1822–1873.
Wu, S., Zhao, X., Li, Y., Du, Q., Sun, J., Wang, Y., et al. (2013). Adsorption properties of doxorubicin hydrochloride onto graphene oxide: Equilibrium, kinetic and thermodynamic studies. *Materials, 6*(5), 2026–2042.
Yan, L., Chang, Y.-N., Zhao, L., Gu, Z., Liu, X., Tian, G., et al. (2013). The use of polyethylenimine-modified graphene oxide as a nanocarrier for transferring hydrophobic nanocrystals into water to produce water-dispersible hybrids for use in drug delivery. *Carbon, 57*, 120–129.
Yang, X., Zhang, X., Liu, Z., Ma, Y., Huang, Y., & Chen, Y. (2008). High-efficiency loading and controlled release of doxorubicin hydrochloride on graphene oxide. *The Journal of Physical Chemistry C, 112*(45), 17554–17558.
Yin, T., Liu, J., Zhao, Z., Zhao, Y., Dong, L., Yang, M., et al. (2017). Redox sensitive hyaluronic acid-decorated graphene oxide for photothermally controlled tumor-cytoplasm-selective rapid drug delivery. *Advanced Functional Materials, 27*(14), 1604620.
Zhang, S., Yang, K., Feng, L., & Liu, Z. (2011). In vitro and in vivo behaviors of dextran functionalized graphene. *Carbon, 49*(12), 4040–4049.
Zuchowska, A., Chudy, M., Dybko, A., & Brzozka, Z. (2017). Graphene as a new material in anticancer therapy-in vitro studies. *Sensors and Actuators B, Chemical, 243*, 152–165.